Phase Separation Process in Poly(ϵ-caprolactone)−Epoxy Blends

Jyh-Luen Chen and Feng-Chih Chang*

Institute of Applied Chemistry, National Chiao Tung University, Hsinchu, Taiwan

Received November 23, 1998; Revised Manuscript Received March 26, 1999

ABSTRACT: Phase separation process in poly(ϵ-caprolactone)−epoxy blends (PCL−epoxy) cured by 4,4′-diaminodiphenyl sulfone (DDS) was investigated by OM and SEM. The blend compositions higher than the critical point exhibit macrophase separation by the spinodal decomposition (SD) mechanism of the epoxy and results in the epoxy particles being dispersed in the matrix. These epoxy particles grow larger gradually and connect to each other to give macrophase epoxy domains with irregular shape. After that, two more stages of microphase separations take place via a nucleation and growth (NG) mechanism and result in smaller epoxy particles being dispersed in the matrix. Blend compositions lower than the critical point exhibit the SD or NG mechanisms of PCL, but the microphase separation is observed only within the epoxy matrix. These phase separation mechanisms can be illustrated successfully by the phase diagram constructed by the spinodal and binodal curves. Hydrogen bonding between protons from the epoxy with carbonyls from PCL has been investigated by FTIR. The mixing free energy reduction by the hydrogen bonding can contribute to the LCST behavior rather than the UCST behavior predicted by the Flory−Huggins equation based on only nonpolar interactions.

Introduction

The miscibility of polymer blends has been a topic of intense interest in polymer science. The major factors influencing polymer miscibility are combinatorial entropy of mixing, interaction energy characterized by the Flory−Huggins interaction parameters, free volume term, and specific interactions such as hydrogen bonding[1]. For nonpolar polymers, the miscibility can be estimated roughly by the Flory−Huggins equation (eq 1), which ignores the free volume term and the specific

$$\frac{\Delta G_N}{RT} = \frac{\phi_1}{N_1} \ln \phi_1 + \frac{\phi_2}{N_2} \ln \phi_2 + \phi_1 \phi_2 \chi \qquad (1)$$

interaction. ΔG_N is the free energy change contributed by the nonpolar interaction. ϕ represents the volume fraction, N is the number of segments in the chain, χ is the interaction parameter calculated by Hilderbrand's solubility parameters, and subscripts 1 and 2 refer to the blending polymers. From this equation at different temperatures, the phase diagram can be derived, which exhibits the upper critical solution temperature (UCST) behavior. The lower critical solution temperature (LCST) behavior can be interpreted by the equation-of-state theory,[2,3] in which the interaction parameter is divided into three parts: segmental interaction, free volume effect, and size effect. This theory is able to interpret both UCST and LCST behaviors. However, the equation-of-state theory cannot be utilized in all cases because these parameters are not all available, especially when these parameters vary during the curing process in thermoplastic/thermoset blends.

Painter et al.[1] suggested adding a term accounting for the free energy of hydrogen-bonding formation into a simple Flory−Huggins expression for the free energy of mixing two polymers:

$$\frac{\Delta G_{mix}}{RT} = \frac{\phi_1}{N_1} \ln \phi_1 + \frac{\phi_2}{N_2} \ln \phi_2 + \phi_1 \phi_2 \chi + \frac{\Delta G_H}{RT} \qquad (2)$$

ΔG_H is the free energy change contributed by the hydrogen bonding between components, which can be estimated by FTIR.[4] This equation ignores the free volume change and other complications, since the aim is to determine an expression in terms of experimentally measurable quantities.

In thermoplastic/thermoset blends, phase transformation has been reported,[5] which involves onset of phase separation, gelation, fixation of the dimension of the phase-separated structure, end of phase separation, and vitrification. When the system is fully gelled, the spacing ceases to increase. Even after gelation, the concentration fluctuation continues to grow further, and the whole system is finally vitrified by the increase in T_g of the epoxy-rich phase. Thus the morphology of a thermoplastic/thermoset blend is determined by the competition of the rates between phase separation and gelation.[6,7] Kim et al.[8] stated that as the cure reaction proceeded, the poly(ether sulfone)/epoxy blend was thrust into the two-phase regime by the LCST depression caused by the increase in molecular weight of the epoxy-rich phase, and the phase separation took place via spinodal decomposition (SD). A binary mixture of the epoxy and amine-terminated butadiene/acrylonitrile liquid rubber (ATBN) exhibits UCST-type phase behavior.[9]

Poly(ϵ-caprolactone) (PCL) is miscible with several amine-cured epoxy resins,[10−12] while two-phase morphology was observed in PCL/anhydride-cured epoxy blends.[11] The observed miscibility difference was interpreted as due to the presence of hydroxyl groups in the amine-cured epoxy. These hydroxyl groups are capable of hydrogen bonding to PCL ester groups. In this study, phase separation process was investigated by optical microscopy (OM) and scanning electron microscopy (SEM). ΔG_H contributed by the hydrogen bonding was estimated by Fourier transform infrared spectroscopy (FTIR). Factors that influence the phase behavior will be discussed later.

Experimental Section

Materials. The epoxy monomer used, DER 332, was purchased from Dow Chemical Co. and is a low molecular weight liquid diglycidyl ether of bisphenol A (DGEBA) with

* To whom correspondence should be addressed.

10.1021/ma981819o CCC: $18.00
Published on Web 07/22/1999

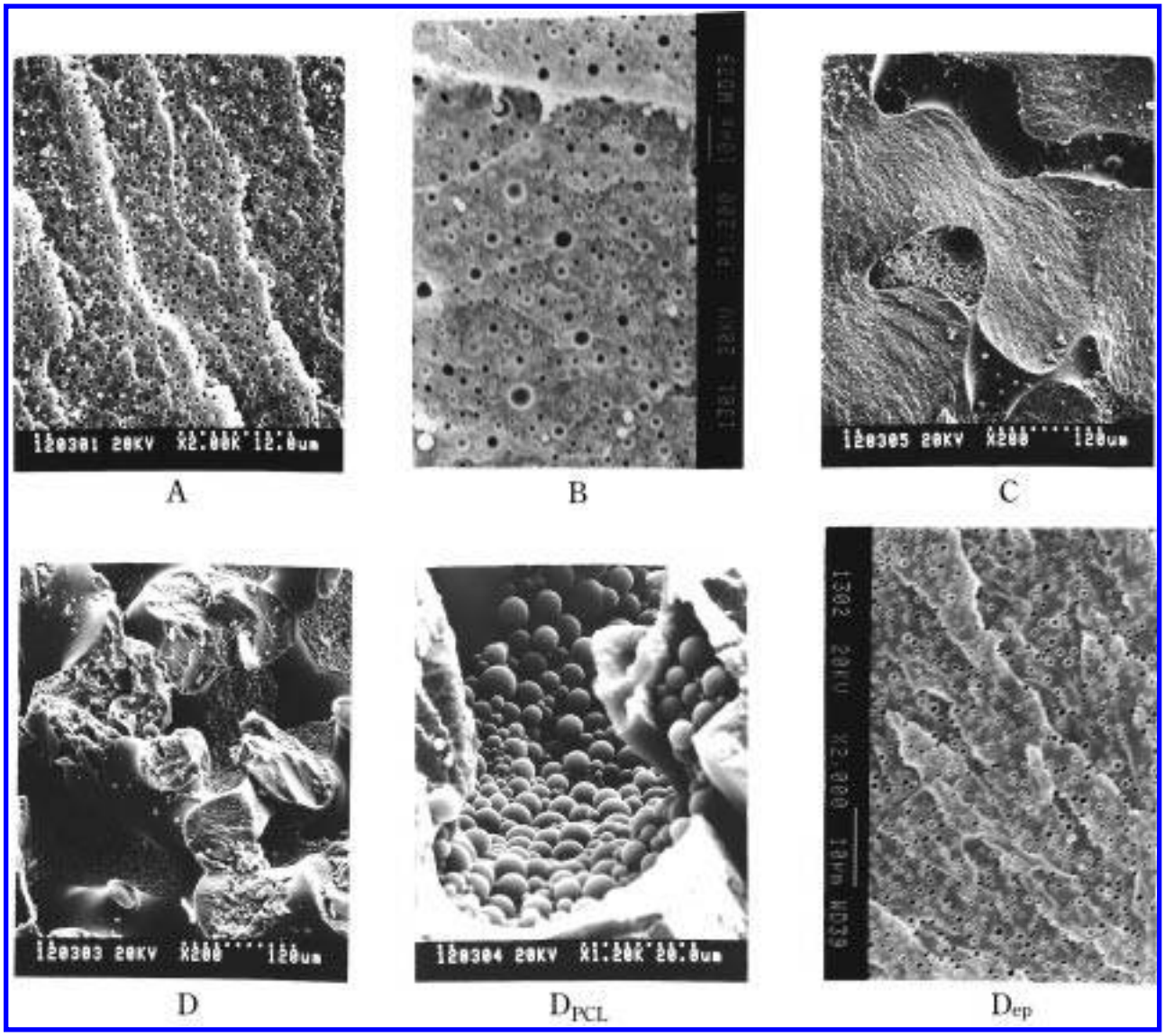

Figure 1. SEM taken on the fractured surfaces of specimens cured at 150 °C for 2 h: (A) PCL 9 wt %; (B) PCL 10 wt %; (C) PCL 12 wt %, (D) PCL 15 wt %; (D_{PCL}) the PCL-rich region of PCL 15 wt %; (D_{ep}) the epoxy-rich region of PCL 15 wt %.

an epoxide equivalent weight of 172−176. PCL used in this study is TONE Polymer P-787 purchased from Union Carbide Corporation with $\bar{M}_n = 80\,000$. The aromatic amine used as a hardener is 4,4′-diaminodiphenyl sulfone (DDS) from Merck Co. The chemical structures of DGEBA, PCL, DDS are illustrated as follows:

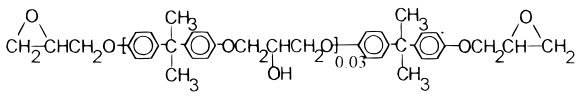

DGEBA (DER 332)

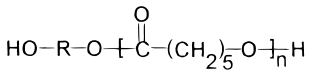

PCL

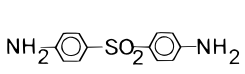

DDS

where "R" represents an aliphatic segment in the PCL structure.

Blending Procedures and Characterizations. The homogeneous mixture of PCL/DGEBA = 30/70 wt % was prepared by adding PCL pellets to the stirring epoxy resin at 150 °C under nitrogen gas for 1 h. After the mixture had cooled to 100 °C, a calculated amount of additional epoxy resin and hardener were added to bring the mixture to the desired composition. The mixture was then cast immediately onto NaCl salt disks, glass slides, and steel molds, respectively. The sample on NaCl salt disks was characterized on a Fourier transform infrared spectrometer (FTIR) (Nicolet 520) in the absorption mode with a resolution of 4 cm^{-1} and heated at 110−170 °C. Spectra were recorded during the whole heating process. The sample on the glass slides was mounted onto a Mettler FP82 hot stage at 150 °C. The phase separation process was observed by optical microscopy (Ziess Axiophot) with time. Hitachi model S-570 and JEOL model JSM 840A scanning electronic microscopes (SEM) were employed to examine morphologies of the fracture surfaces of specimens cured at 150 °C. The reaction heats from the heating scan and three isothermal reactions were obtained by a DSC 910S differential scanning calorimeter (DSC) from TA Instruments. The total reaction heat was obtained by a heating scan using a 5 °C/min heating rate from room temperature to 300 °C. The conversions in three isothermal reaction temperatures were also estimated at 175, 185, and 195 °C, respectively. The reaction rate equation in the autocatalytic mode can be calculated from the above results.

Results and Discussion

Morphologies. SEM morphologies of fractured surfaces of four finally cured compositions are shown in Figure 1. The blend, PCL/DGEBA/DDS = 9/67.5/22.5 (PCL 9 wt %), displays a spherical dispersed PCL-rich

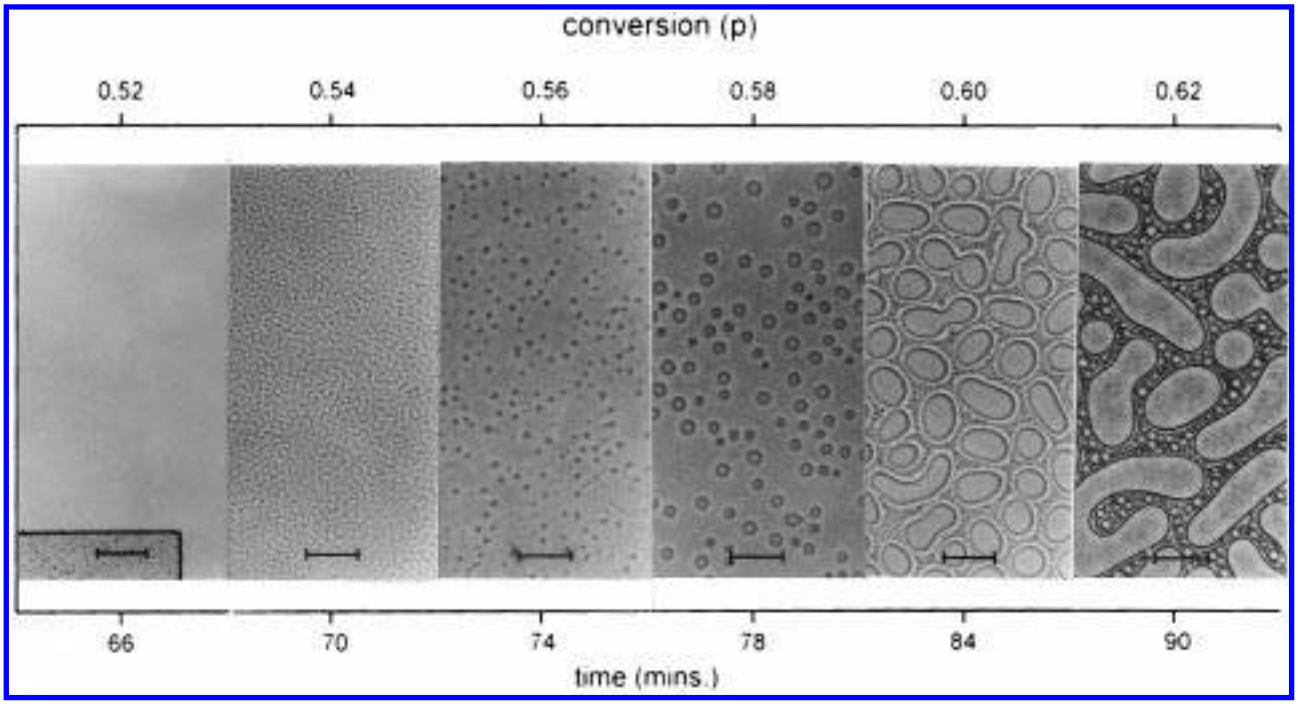

Figure 2. OM taken on PCL 15 wt % pasted between slides heated at 150 °C. The length of the short bar is 31.25 μm.

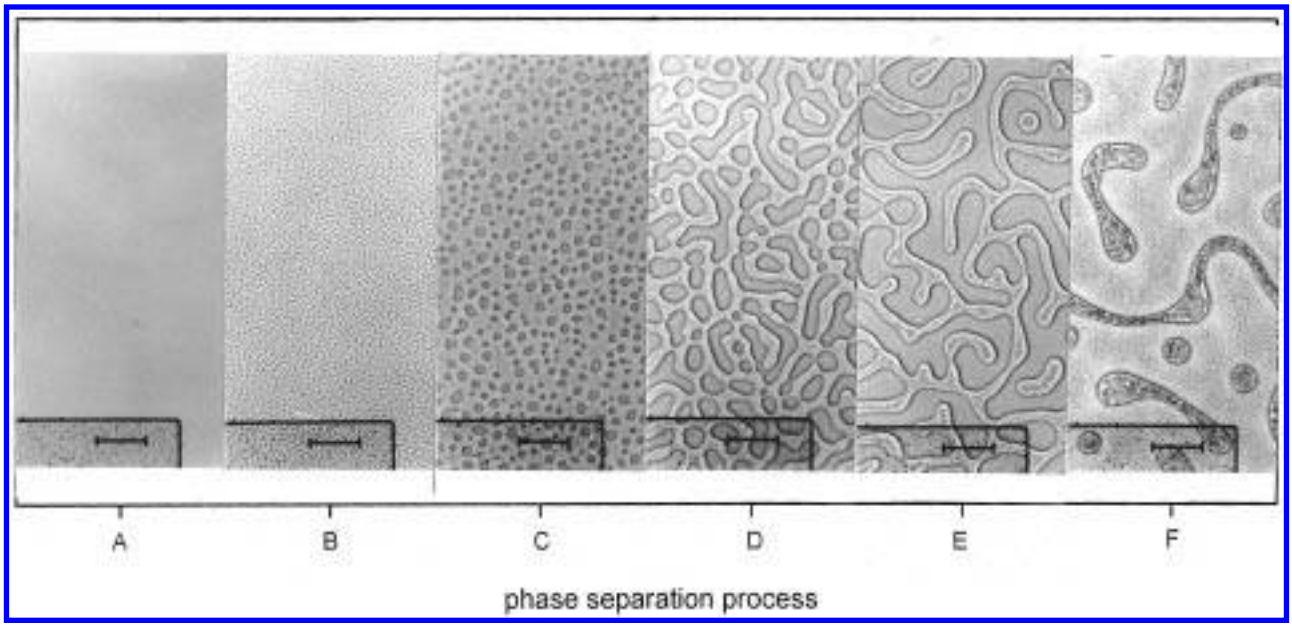

Figure 3. OM taken on PCL 12 wt % pasted between slides heated at 150 °C. The length of the short bar is 31.25 μm.

(epoxy-lean) phase as shown in Figure 1A, while the PCL 10 wt % blend (Figure 1B) displays a similar dispersed phase of different sizes. The weight ratio of DGEBA/DDS remains as 3 in all compositions. Figure 1C (PCL 12 wt %) displays an irregular shape of the PCL-rich phase dispersed in the matrix, which is in contrast to Figure 1D (PCL 15 wt %) because the PCL-rich phase inverts to the matrix. The SEM micrographs at a higher mignification taken on both the PCL-rich (Figure 1D$_{PCL}$) and epoxy-rich (Figure 1D$_{ep}$) regions of the PCL 15 wt % blend illustrate the morphologies in detail, which are similar to those of the PCL 12 wt % blend. The appearance of these smaller visible particles (epoxy) in the etched phase (Figure 1D$_{PCL}$) implies that second and possible third stage of microphase separation continues to proceed after the primary macrophase separation. On the other hand, smaller PCL-rich particles are etched in the epoxy-rich region (Figure 1D$_{ep}$), and no further epoxy particles are observed within these etched particles. The morphological variation within the blends of PCL 9−15 wt % implies that the critical point on the phase diagram should be located in this region.

Figures 2−5 display OM micrographs of four different compositions which illustrate the phase separation process. The micrographs in Figure 2 show the phase separation process of the PCL 15 wt % blend heating at 150 °C with respect to time and conversion calculated by the reaction rate equation:

$$\frac{dp}{dt} = k(1-p)^{1.66}p^{0.144} \tag{3}$$

$$k = Z\exp\left(-\frac{E_a}{RT}\right) \tag{4}$$

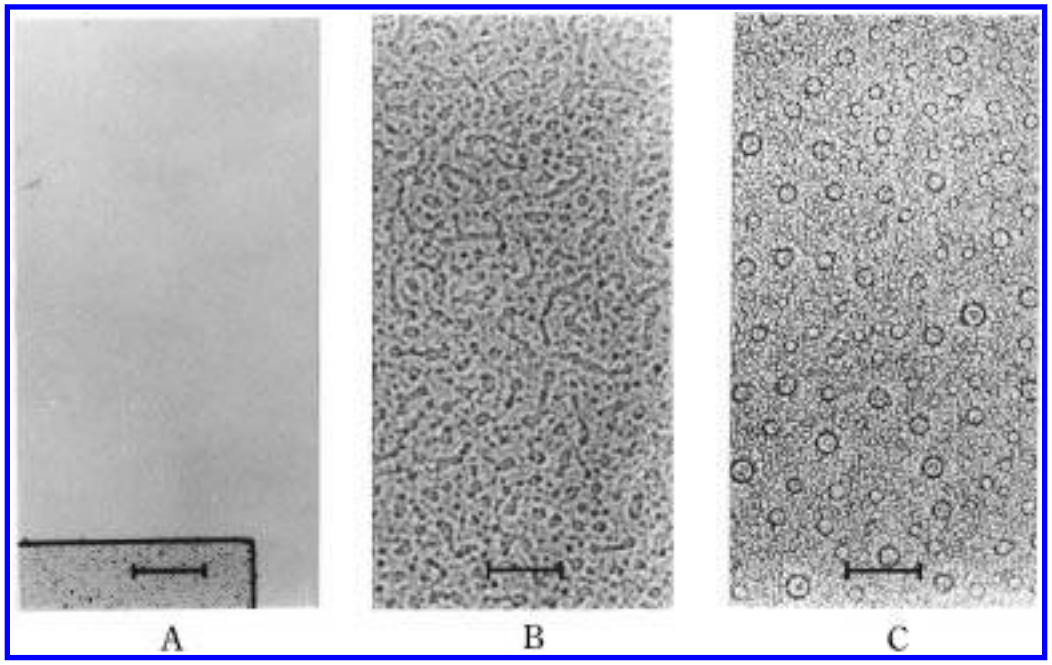

Figure 4. OM taken on PCL 10 wt % pasted between slides heated at 150 °C. The length of short bar is 31.25 μm.

where p, t, and k are the conversion, reaction time, and reaction rate constant, respectively. Z is the collision factor ($\log Z = 8.10\ \text{min}^{-1}$), E_a is the activation energy ($E_a = 79.8$ kJ/mol), and T is the reaction temperature. The PCL 15 wt % blend remains homogeneous after 66 min at 150 °C. The co-continuous morphology at 70 min indicates that the phase separation takes place via a SD mechanism. The co-continuous structure shifts gradually into small epoxy-rich dispersed particles (70 → 74 min). The size of these small dispersed particles grows gradually (74 → 78 min). These growing particles connect to each other to form large particles (78 → 84 min). It is interesting to find out that finer particles start to appear and disperse in the continuous phase. After 90 min, the morphology is finally fixed in which irregular macrophase domains are dispersed in the matrix while the fine particles distributed in the matrix from later stages of phase separation are present. Additionally, many smaller spherical PCL-rich particles in the epoxy-rich phase can also be identified by Figure 1D$_{ep}$. From the OM micrographs shown in Figure 3, the phase separation of the PCL 12 wt % blend takes place in the same manner as that in the PCL 15 wt % blend except that the phase inversion occurs. The epoxy-dispersing phase grows further and becomes more interconnected and eventually becomes the continuous phase (Figure 3D → Figure 3E). In this PCL 12 wt % blend, the fine epoxy particles are distributed within the dispersed PCL-rich phase (Figure 3E → Figure 3F). Comparing the final morphologies observed by SEM (Figure 1C,D) to OM (Figure 2, 90 min, and Figure 3F), it is interesting to notice that these small particles appearing in the early stage of phase separation (Figure 2, 74 min, and Figure 3C) are the epoxy particles. Although the PCL content is substantially less than that of the epoxy, the macrophase separation results in smaller epoxy particles dispersing in the matrix. However, the final morphology is dictated by the PCL content. Phase inversion in the separation process results in epoxy as the matrix when the PCL content of the blend is 12 wt %. The macrophase separation process of the PCL 15 wt % blend is similar to the mechanism proposed by Yamanaka and Inoue.[13] They reported that phase separation takes place via SD induced by the increase in the epoxy molecular weight. Then the epoxy-rich droplets resulting from SD grow further and finally contact and connect to each other to yield the connected-globule structure. The epoxy-rich droplets remain as individuals and connect to each other with a little contact, while the irregular shape of the epoxy phase is formed in this study (Figures 1−3). However, microphase separations during later stages do not occur in their report.

Figures 4 and 5 display the phase separation process of PCL 10 wt % and PCL 9 wt % blends, respectively. The micrographs in Figure 4 illustrate a SD mechanism (Figure 4B), but the co-continuous structure is thrust into the PCL-rich phase dispersed in the epoxy-rich matrix (Figure 4C), which is in contrast to the results of the PCL 15 wt % blend (Figure 2, 74 min) and the PCL 12 wt % blend (Figure 3C), for many small particles are present in the matrix at the same time. Thus the critical point of drastic change in phase diagram should be located at PCL 11 wt % composition. The micrographs of the PCL 9 wt % blend (Figure 5) do not display a typical SD mechanism. Many tiny points appear in the early stage of phase separation (Figure 5B), and the point density increases with time (Figure 5C). Compared to the SEM micrograph of the PCL 9 wt % blend (Figure 1A), the nucleation and growth (NG) mechanism of PCL should be obeyed in the epoxy-rich phase of all four compositions.

Figure 6 illustrates the phase changes of the PCL 12 wt % blend by varying temperatures. The sample is heated at 150 °C until the co-continuous phase appears (Figure 6A). When this specimen is cooled to 80 °C by 30 °C/min cooling rate and is maintained isothermally at 80 °C for 5 min (Figure 6B), the boundary between phases is blurred and becomes nearly homogeneous. When the sample is reheated to 150 °C with the expected higher conversion (Figure 6C), the phase boundary of the co-continuous morphology even exceeds that before cooling as shown in Figure 6A. The conversion difference between these micrographs (Figure 6A and Figure 6C) is probably insignificant because of the poor reactivity of DDS under this condition. This

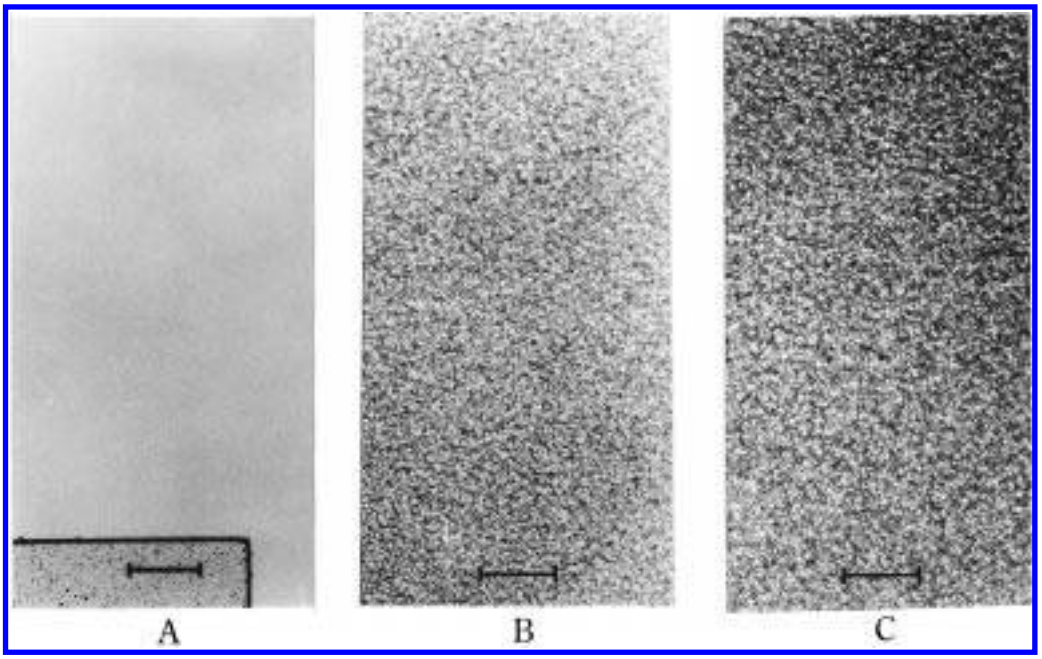

Figure 5. OM taken on PCL 9 wt % pasted between slides heated at 150 °C. The length of short bar is 31.25 μm.

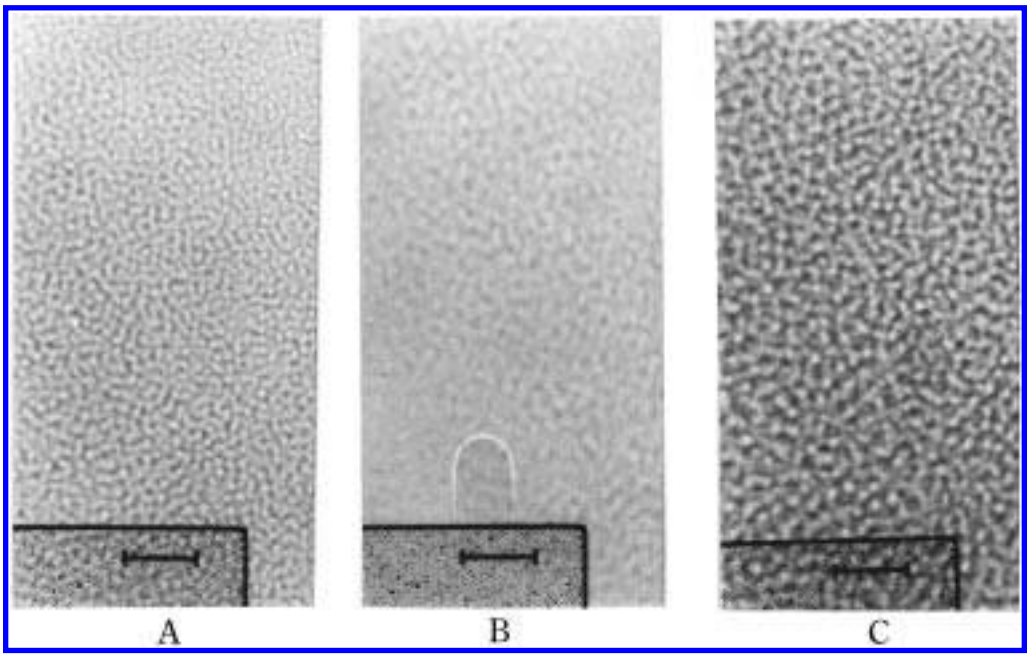

Figure 6. OM taken on PCL 12 wt % pasted between slides (A) heated at 150 °C, (B) cooled to 80 °C, and (C) heated again to 150 °C. The length of the short bar is 31.25 μm.

phenomenon suggests that the miscibility of this system is improved at a lower temperature, and a LCST behavior is expected.

Molecular Weight of the Epoxy. Flory[14] proposed an equation of a 3-dimensional number- and weight-average degree of polymerization ($\bar{X}_n$, $\bar{X}_w$) with respect to conversion (p), functionality of the branch units ($f = 4$), branching coefficient ($\alpha = p^2$). $\bar{X}_n$ and $\bar{X}_w$ can be given by the following equations:

$$\bar{X}_n = \frac{1}{1 - (\alpha f/2)} = \frac{1}{1 - 2p^2} \tag{5}$$

$$\bar{X}_w = \frac{1 + \alpha}{1 - (f - 1)\alpha} = \frac{1 + p^2}{1 - 3p^2} \tag{6}$$

In this system the number- and weight-average molecular weights of the unreacted monomers are $\bar{M}_{n0} = 315$ g/mol and $\bar{M}_{w0} = 322$ g/mol. Therefore, the number- and weight-average molecular weight ($\bar{M}_n$, $\bar{M}_w$) can be expressed by the following equations:

$$\bar{M}_n = \bar{M}_{n0}\,\bar{X}_n = \frac{315}{1 - 2p^2} \tag{7}$$

$$\bar{M}_w = \bar{M}_{w0}\bar{X}_w = \frac{322(1 + p^2)}{1 - 3p^2} \tag{8}$$

Both $\bar{M}_n$ and $\bar{M}_w$ are calculated and plotted in Figure 7. When $P > 0.5$, the $\bar{M}_w$ increases at a faster rate than that of the $\bar{M}_n$, an indication of a drastic increase in the polydispersity. This phenomenon indicates that a great number of low molecular weight (MW) monomers and oligomers are still present at this stage of conversion.

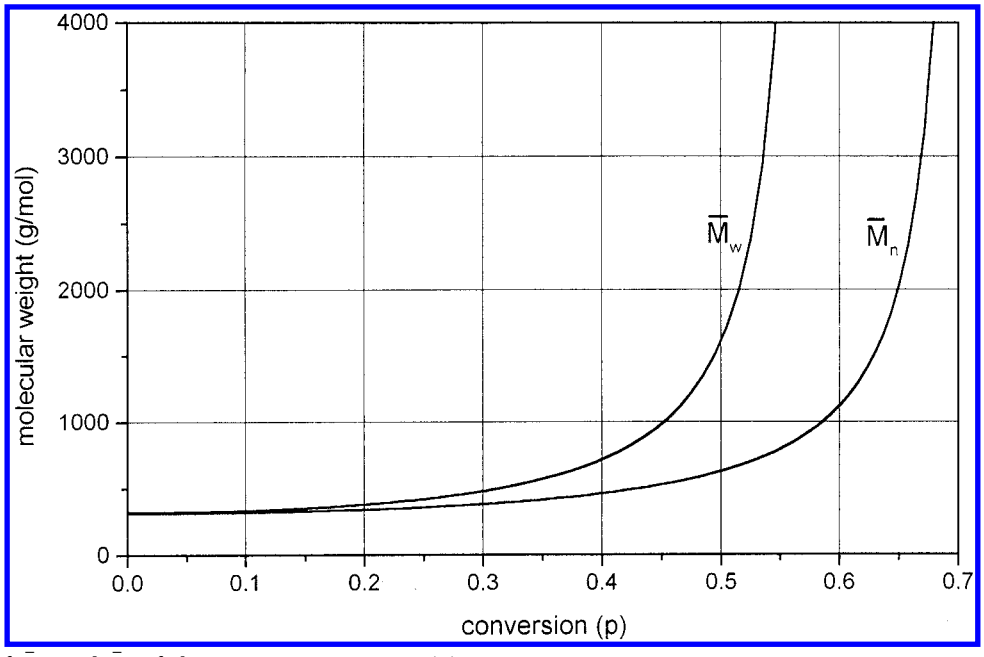

Figure 7. Plot of $\bar{M}_w$ and $\bar{M}_n$ of the epoxy vs conversion (P).

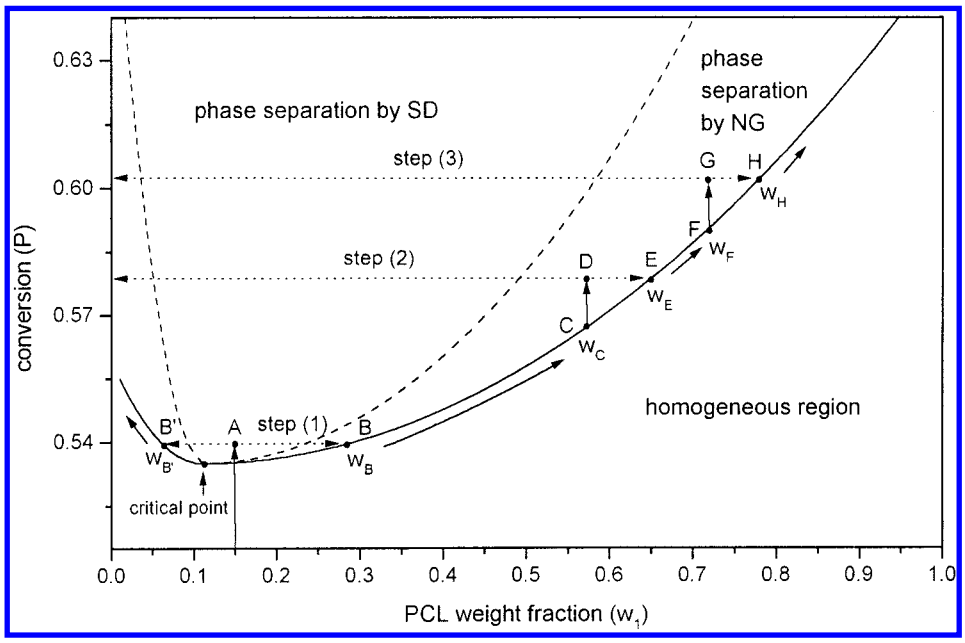

Figure 8. Phase diagram of the conversion (P) vs weight fraction of PCL (w_1)

The phase separation of PCL 15 wt % blend proceeds from $p = 0.52-0.62$ (Figure 2), in other words, $\bar{M}_n = 686-1362$ and $\bar{M}_w = 2167$ to infinity (Figure 7). In the early stages of phase separation, those epoxy molecules with higher MW are segregated from the matrix. Those epoxy molecules with lower MW still soluble in the matrix exhibit greater mobility and better miscibility with PCL continue to grow further. When the $\bar{M}_w$ approaches infinity ($p > 0.577$), the central region of the epoxy-rich phase has gelled, but the phase domains continue to grow. Those lower MW epoxies close to the phase boundary can still diffuse into the epoxy-rich domains; thus the average gel point ($p = 0.577$) cannot be defined as the end point of phase separation.

Phase Separation Mechanism. The phase separation processes in both PCL 15 and 12 wt % can be interpreted in the same way through the phase diagram proposed in Figure 8, which is similar to that in the report of Williams et al.[16] The initial compositions (PCL 12 and 15 wt %) are located at the right-hand side of the critical point (PCL 11 wt %), because the phase separations are initiated from the epoxy-rich phases. Three steps of phase separations according to Figure 2 are labeled in Figure 8 to illustrate the phase separation process. When the epoxy conversion is increased to a point above spinodal and binodal curves (Figure 8, point A), phase separation initiates by the SD mechanism (step 1). Since the difference between spinodal and binodal curves is insignificant, it is reasonable to assume that the epoxy conversion jumps over the binodal curve (Figure 8, point A) to initiate via the SD mechanism. The composition is divided into two compositions after phase separation, $w_1 = w_B$ and $w_1 = w_{B'}$ (Figure 8, points B and B′) corresponding to the micrographs taken at 66−74 min in Figure 2. The co-continuous structure quickly turns into small and evenly distributed epoxy droplets as shown in the micrographs taken at 70−74 min in Figure 2, as well

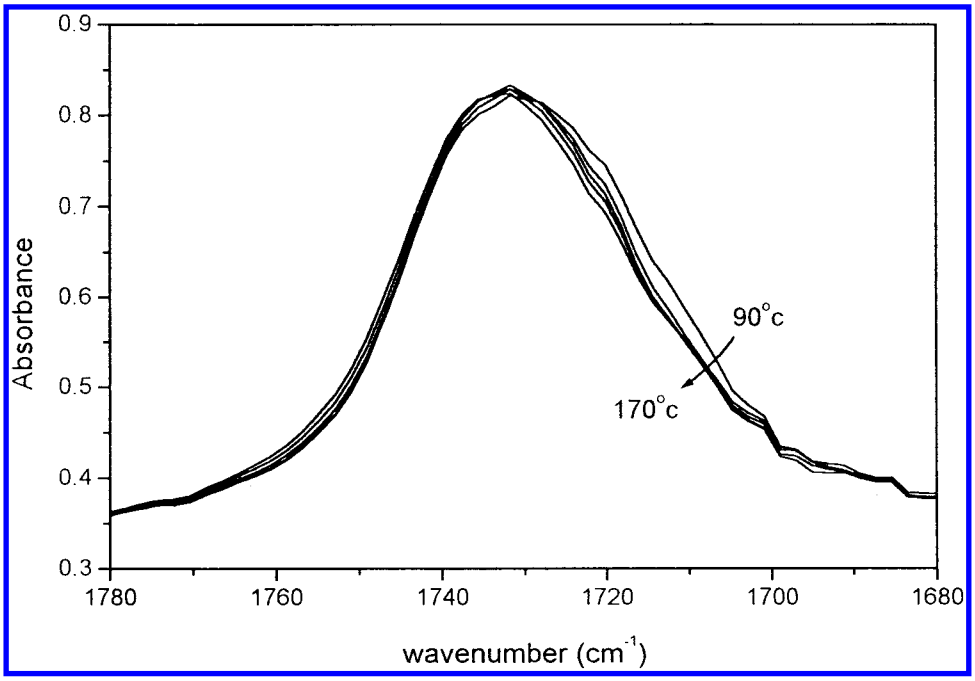

Figure 9. FTIR spectrum of PCL 32.5 wt % at $P = 0.3$ heated at 90−170 °C, respectively, in the carbonyl stretching region (1780−1680 cm^{-1}).

as points B and B′ of Figure 8. We believe that these phase-separated epoxy particles possess higher average molecular weights than those still in the matrix solution. Phenomenologically, the phases grow and coalesce with each other to form larger particles from this moment on by following the binodal curve of B→C of Figure 8 corresponding to Figure 2, 74→78 min. The epoxy concentration in these epoxy droplets ($w_2 > 1 - w_{B'}$) is higher than that in the matrix between $w_2 = 1 - w_B$ and $1 - w_C$; therefore, the epoxy curing rate is expected to be higher than that in the matrix. Higher epoxy conversion in the epoxy phase results in higher epoxy molecular weight and the formation of the lightly cross-linking structure; thus the solubility with the relatively lower molecular weight epoxy in the matrix becomes poorer. That means that taking epoxy molecules from the matrix into these phase separated epoxy particles becomes more difficult. On the other hand, the viscosity of the matrix at point C ($w_1 = w_C$) also increases; thus the long-distance diffusion of the epoxy molecules far from the phase boundary into the epoxy macrophase becomes difficult or even impossible. Additionally, the epoxy molecules in the matrix again become immiscible with PCL in the matrix due to the growth of the epoxy molecular weight so that they have to seek another means of phase segregation. When the concentration of these higher molecular weight epoxies grows to a critical level (Figure 8, point D), a new phase separation via the NG mechanism proceeds following the step 2 microphase separation path D−E corresponding to the micrograph taken at 84 min in Figure 2. The micrograph taken at 84 min in Figure 2 clearly shows the appearance of numerous tiny particles within the matrix while the coalescence of the macrophase continues. Phase growth in step 2 microphase separation proceeds via the NG mechanism through the route of E−F until approaching point F. In this time period (E→F), the epoxy macrophase grows by the entry of the dissolved epoxy and the tiny epoxy particles close to the phase boundary (Figure 2, 84→90 min). Similar to the situation at the end of step 1, the diffusion of the dissolved epoxy far from the phase boundary of tiny epoxy particles becomes more difficult at the end of step 2 for the same reasons as that described in step 1. Hence step 3 phase separation occurs in a manner similar to that of step 2 by the route of F−G−H. The distance between the tiny particles segregated in step 3 is shorter than that in step 2, because the higher conversion in step 3 leads to shorter diffusion allowed and poor miscibility. The expected size of the particles produced via step 3 process should be substantially smaller than that from those of step 2. The micrograph taken at 90 min in Figure 2 shows that the size of the step 2 grown particles are above the mean (6.2 μm diameter). An SEM micrograph of Figure $1D_{PCL}$ shows that the phase is composed mainly of the larger particles with dimensions similar to those from OM (Figure 2, 90 min). Besides those relatively larger particles shown in Figure $1D_{PCL}$, various smaller particles (2.2 μm diameter) are also present that provide the evidence for step 3 (or possibly step 4) phase separation. On the other hand, the epoxy concentration in the growing epoxy-rich phase increases continuously and follows the binodal curve in the left-hand side of the critical point through all steps. The solubility in the epoxy-rich phase gets worse with the increase of the epoxy conversion, and the microphase separation takes place via a NG mechanism of PCL, which is confirmed by the etched particles in Figure $1D_{ep}$ and tiny points within the epoxy macrophase in Figure 2, 90 min. This microphase separation can be illustrated in the manner described above.

The phase separation processes of the PCL 10 and 9 wt % blends can also be illuminated by the phase diagram in a similar manner as those of the PCL 15 and 12 wt % blends. The PCL-rich phase segregates from the matrix in both compositions located at the left-hand side of the critical points. After the SD mechanism of PCL in the PCL 10 wt % blend, the microphase separation takes place in the epoxy-rich phase but not in the PCL-rich phase (Figure 1B and Figure 4C), because the longer distance of diffusion in the epoxy-rich phase is inhibited by the higher viscosity and worse

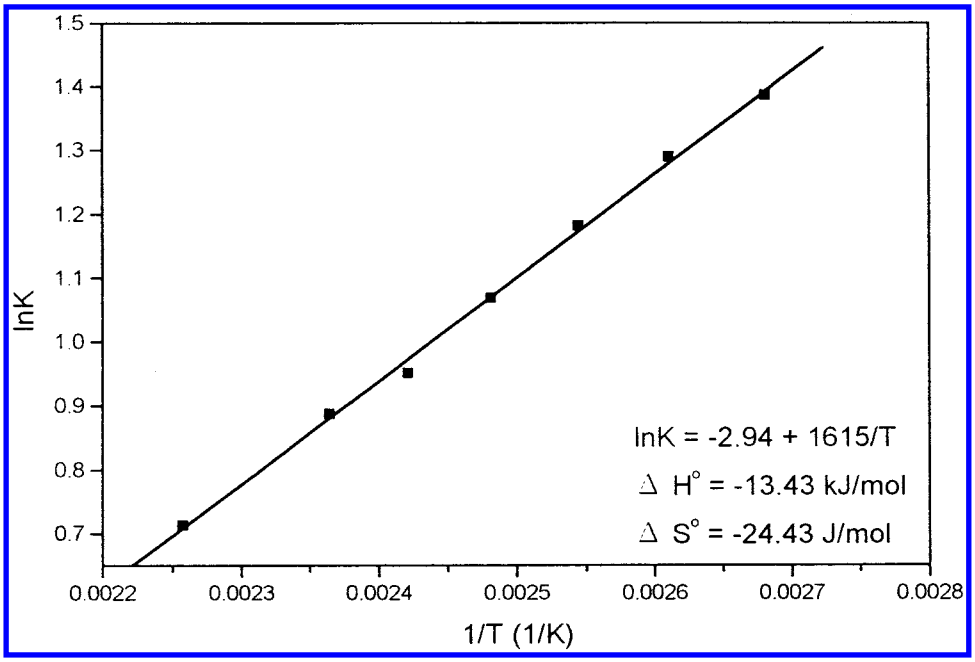

Figure 10. Plot of ln K vs $1/T$ of PCL 32.5 wt %.

Table 1. Analysis Results of PCL 32.5 wt % for the Peaks of Carbonyls in the FTIR Spectrum

T (°C)	$\%A_{1727}/\%A_{1736}$	α_{eq}[a]	K	ΔG_H (J/mol)[b]
170	55.6/44.4	0.50	2.04	0
150	58.4/41.6	0.53	2.43	−662
140	59.5/40.5	0.54	2.59	−935
130	61.1/38.9	0.56	2.91	−1396
120	62.7/37.3	0.58	3.26	−1854
110	64.4/35.6	0.60	3.63	−2313
100	65.7/34.3	0.61	4.00	−2607

[a] The ratio of extinction coefficients of hydrogen-bonding to free carbonyls is 1.23.[17] [b] Per mole of carbonyls.

miscibility at higher epoxy conversion. In the meantime, the epoxy in the PCL-rich phase has a lower conversion than that in the matrix and thus better miscibility with PCL. The shorter distance of diffusion also promotes the PCL concentration without the microphase separation. The PCL 9 wt % composition locates in the region of the NG mechanism of PCL, and thus a simple morphology is observed. The epoxy does not segregate from the PCL-rich particles that can be interpreted as being due to the same reason described for the PCL 10 wt % blend.

Hydrogen Bonding. The blend containing 32.5 wt % PCL gives the stoichiometric carbonyls relative to the protons from the sum of amine and hydroxyl. FTIR spectra in the carbonyl stretching region (1780−1680 cm^{-1}) are shown in Figure 9 with respect to various temperatures at same epoxy conversion (P = 0.3) estimated by the absorption of the epoxide (910 cm^{-1}). These curves can be divided into two groups representing free and hydrogen-bonded carbonyls. It can be expressed as an equilibrium as the following

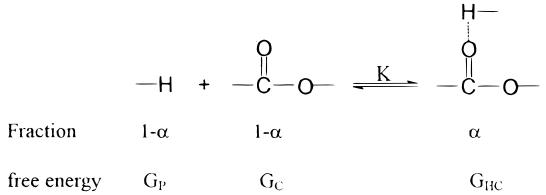

where K is the equilibrium constant and α is the fraction of hydrogen-bonded carbonyls. G_P, G_C, and G_{HC} are molar free energies of these protons, free carbonyl, and hydrogen-bonded carbonyl, respectively. The calculated results for the fraction of hydrogen-bonded carbonyl are listed in Table 1, and the equilibrium constants are calculated by $K = \alpha/(1-\alpha)^2$. The equilibrium constant K and the free energy change of this system at $P = 0.3$ can be expressed as

$$\Delta G = \Delta G° + RT \ln K \tag{9}$$

When the equilibrium is reached, $\Delta G = 0$; hence the equilibrium constant K can be estimated by

$$\ln K = -\frac{\Delta G°}{RT} = -\frac{\Delta H°}{RT} + \frac{\Delta S°}{R} \tag{10}$$

$\Delta H°$ and $\Delta S°$ are obtained from the intercept and the slope in the plot of ln K vs $1/T$ shown in Figure 10. The free energy change can be expressed as

$$\Delta G = 0 = \alpha_{eq} G_{HC} - (1-\alpha_{eq})(G_P + G_C)$$

where $\alpha_{eq} = 0.53$ at 150 °C (Table 1); thus

$$0.53 G_{HC} - 0.47(G_P + G_C) = 0 \tag{11}$$

When $K = 1$ and $\alpha = 0.38$, the free energy change at T = 150 °C is

$$\Delta G = \Delta G°$$

$$\alpha G_{HC} - (1-\alpha)(G_P + G_C) = \Delta H° - T\Delta S°$$

$$0.38 G_{HC} - 0.62(G_P + G_C) = -3.09 \text{ kJ/mol} \tag{12}$$

From eqs 12 and 13, we obtain G_{HC} = 9.83 kJ/mol, and $G_P + G_C$ = 11.08 kJ/mol. The free energy change per mole of carbonyl resulting from hydrogen bonding can be estimated as

$$\Delta G_H = [\alpha G_{HC} + (1-\alpha)(G_P + G_C)] - [1*(G_P + G_C)] = -662 \text{ J/mol} \tag{13}$$

The last term in eq 2 ($\Delta G_H/RT$) represents the free energy change per mole of lattice cell contributed by the hydrogen bonding. The ΔG_H per mole of carbonyls can also be calculated at different temperatures (Table 1) by the similar method described in eqs 12 and 13. ΔG_H increases with the increase in temperature, which indicates that hydrogen bonding should contribute to the LCST behavior, which is confirmed by OM (Figure 6).

Conclusions

The macrophase separation mechanism depends on the blend compositions, while the microphase separation takes place via the NG mechanism regardless of the initial compositions. Both macro- and microphase separation processes can be illustrated by the phase diagram. After the SD mechanism of the epoxy in the blend compositions (PCL 15 and 12 wt %) becomes higher than the critical point (PCL 11 wt %), the epoxy particles are dispersed in the matrix and grow gradually to give the epoxy macrophase with irregular shape. When the epoxy molecules remaining in the matrix become insoluble, primary microphase separation takes place via the NG mechanism and results in smaller epoxy particles dispersed between the epoxy macrophases. Further microphase separation occurs for the same reasons and results in even smaller epoxy particles. Additionally, the microphase separation by the NG mechanism of PCL is also present inside the epoxy macrophase.

When the blend composition (PCL 10 wt %) is a little lower than the critical point, the SD mechanism of PCL proceeds and is followed by the NG mechanism of PCL in the epoxy matrix. The epoxy microphase is absent within the PCL macrophase, because the diffusion of the epoxy is not inhibited and the microphase separation is unnecessary. The phase separation initiated by the NG mechanism of PCL can be illustrated by a similar method (PCL 9 wt %). Hydrogen bonding between protons from the epoxy with carbonyls from PCL contributes to the LCST behavior rather than as UCST behavior predicted by the Flory−Huggins equation based on only nonpolar interactions.

Acknowledgment. This research is financially supported by the National Science Council, Taiwan, R.O.C. under Contract No. NSC 87-2216-E-009-007. We thank Epolab Chemical Co. for donation of material.

References and Notes

(1) Painter, P. C.; Park, Y.; Coleman, M. M. *Macromolecules* **1988**, *21*, 66.
(2) Kammer, H. W.; Inoue, T.; Ougizawa, T. *Polymer* **1989**, *30*, 888.
(3) Kammer, H. W.; Kressler, J.; Kummerloewe, C. *Adv. Polym. Sci.* **1993**, *106*, 31.
(4) Lee, J. Y.; Painter, P. C.; Coleman, M. M. *Macromolecules* **1988**, *21*, 346.
(5) Kim, B. S.; Chiba, T.; Inoue, T. *Polymer* **1993**, *34*, 2809.
(6) Verchere, D.; Sautereau, H.; Pascault, J.-P.; Moscliar, S. M.; Riccardi, C. C.; Williams, R. J. J. *Toughened Plastics I*; American Chemical Society: Washington, DC, 1993; p 335.
(7) Teng, K. C.; Chang, F. C. *Polymer* **1993**, *34*, 4291.
(8) Kim, B. S.; Chiba, T.; Inoue, T. *Polymer* **1995**, *36*, 67.
(9) Yamanaka, K.; Takagi, Y.; Inoue, T. *Polymer* **1989**, *60*, 1839.
(10) Chen, J. L.; Huang, H. M.; Li, M. S.; Chang, F. C. *J. Appl. Polym. Sci.* **1999**, *71*, 75.
(11) Clark, J. N.; Daly, J. H.; Garton, A. *J. Appl. Polym. Sci.* **1984**, *29*, 3381.
(12) Garton, A. *Polym. Eng. Sci.* **1983**, *23*, 663.
(13) Yamanaka, K.; Inoue, T. *Polymer* **1989**, *30*, 662.
(14) Flory, P. J. *Principles of Polymer Chemistry*; Cornell University Press: Ithaca, NY, 1953, Chapters 3, 8, and 9.
(15) Oyanguren, P. A.; Riccardi, C. C.; Williams, R. J. J.; Mondragon, I. *J. Polym. Sci., Part B: Polym. Phys.* **1998**, *36*, 1349.
(16) Williams, R. J. J.; Rozenberg, B. A.; Pascault, J.-P. *Adv. Polym. Sci.* **1997**, *128*, 95.
(17) Garton, A. *Polym. Eng. Sci.* **1984**, *24*, 112.

MA981819O